Electronic supplementary information for

Luminescent 2D single crystals of thiophene-phenylene co-oligomers for field-effect devices

Roman S. Fedorenko[a,b], Alexey V. Kuevda[a,b,c], Vasiliy A. Trukhanov[a,b], Andrey Yu. Sosorev[a,b], Artem V. Bakirov[b,d], Artem I. Dorokhov[a], Nicolay M. Surin[b], Oleg V. Borshchev[b], Sergey A. Ponomarenko*[b], Dmitry Yu. Paraschuk**[a,b]

[a] Faculty of Physics, Lomonosov Moscow State University, Leninskie Gory 1/62, Moscow 119991, Russia

[b] Enikolopov Institute of Synthetic Polymeric Materials, Russian Academy of Sciences, Profsoyuznaya Str. 70, Moscow 117393, Russia

[c] Skolkovo Institution of Science and Technology, Bolshoy Bulvar 30, Moscow Oblast, 143026, Russia

[d] National Research Centre "Kurchatov Institute"; 1 Kurchatov sq., Moscow, 123098, Russia

* E-mail: ponomarenko@ispm.ru

**E-mail: paras@physics.msu.ru

Table of contents

1. Calculations

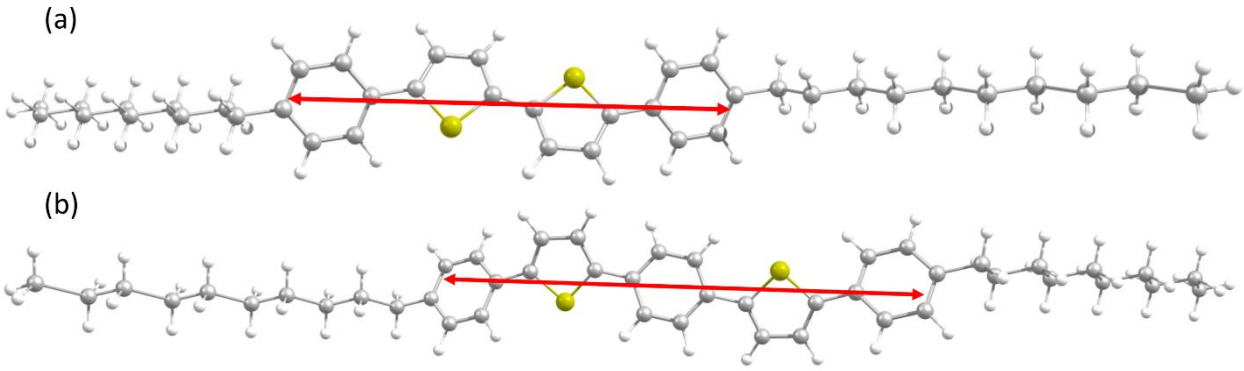

Figure S1. Calculated transition dipole moments (TDMs) for DD-PTTP (a) and DD-PTPTP (b); they form the angles of 4.5° and 4.7° with the molecular axes, respectively.

a)

b)

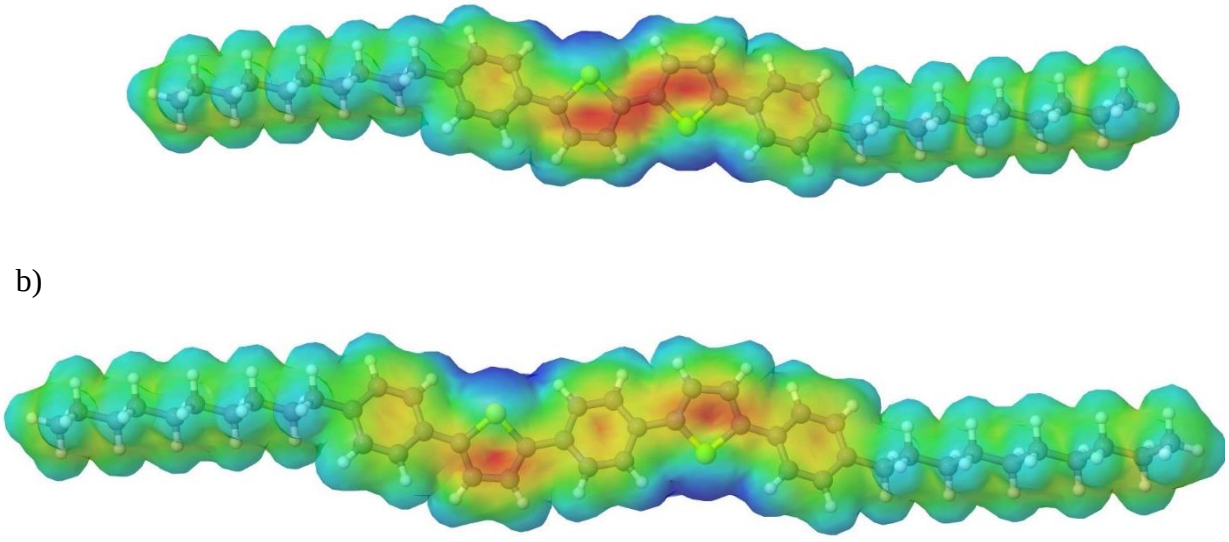

Figure S2. Ground-state electrostatic potential for DD-PTTP (a) and DD-PTPTP (b).

Table S1. HOMO-LUMO/optical gaps and geometrical parameters of DD-PTTP and DD-PTPTP calculated with and without Grimme's D3 empirical correction.

	Approximation	HOMO-LUMO gap	E_g^{abs}, eV	P-T torsional angle, degrees	P-T interring bond, Å
DD-PTTP	B3LYP/6-31g(d,p)	3.37	3.09	25.9	1.47
	B3LYP-D3/6-31g(d,p)	3.38	3.09	27.3	1.47
DD-PTPTP	B3LYP/6-31g(d,p)	3.45	3.11	23.7 (central); 30.8 (peripheric)	1.46 (central); 1.47 (peripheric)
	B3LYP-D3/6-31g(d,p)	3.50	3.15	27.1 (central); 30.2 (peripheric)	1.46 (central); 1.47 (peripheric)

2. NMR and mass spectra

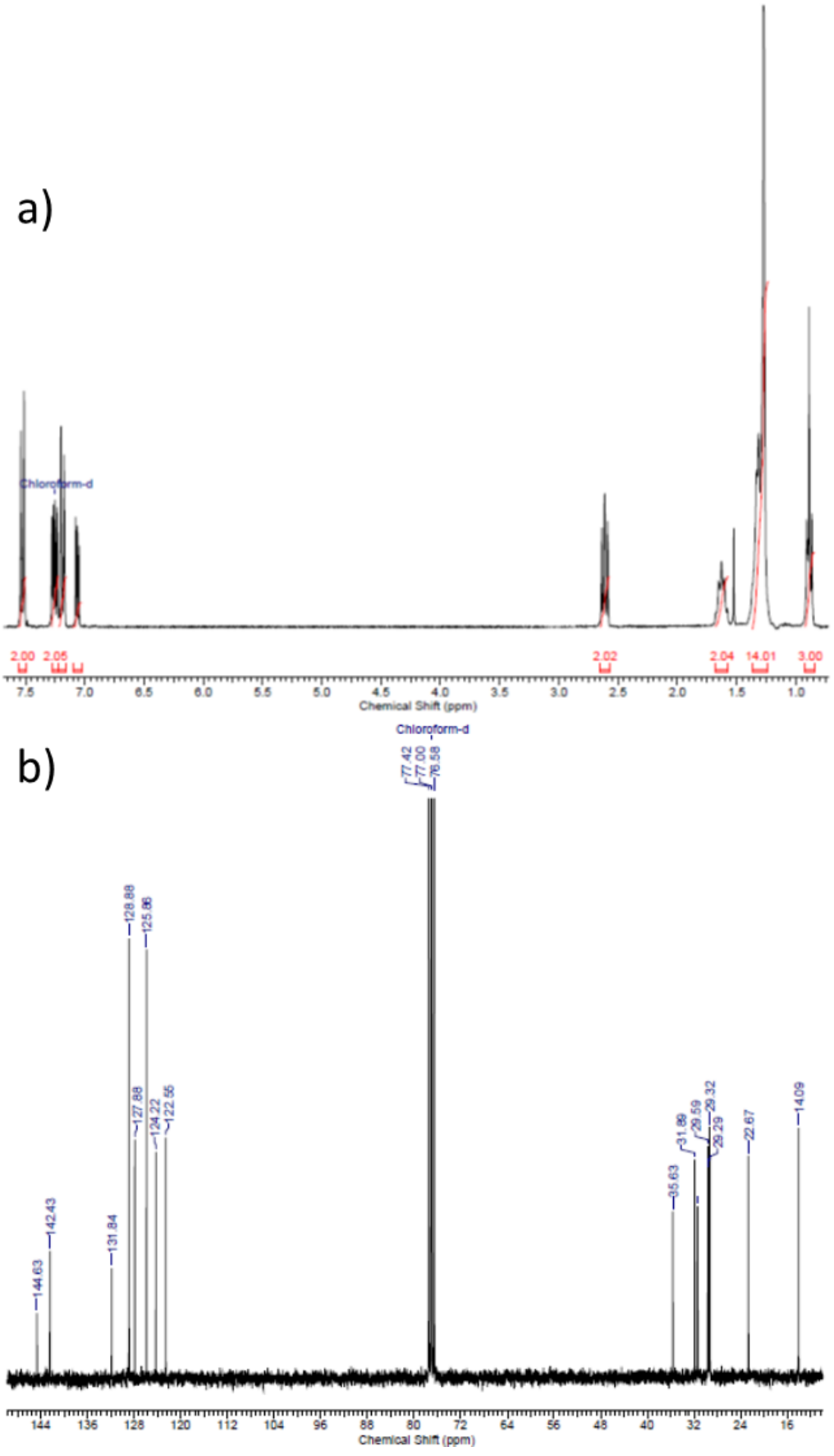

Figure S3. ^{1}H NMR (a) and ^{13}C NMR (b) spectrum of 2-(4-decylphenyl)thiophene (D-PT).

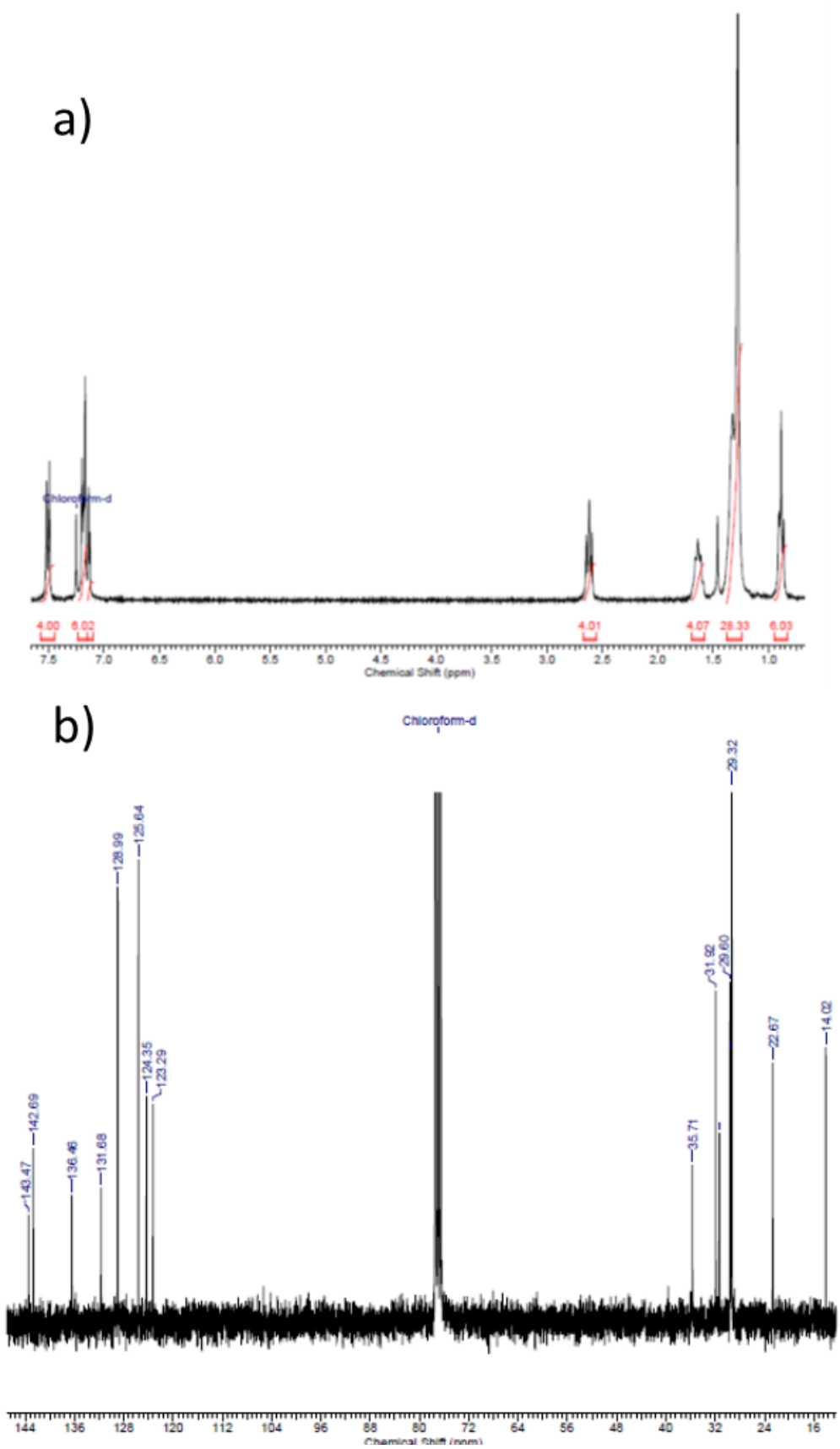

Figure S4. ^{1}H NMR (a) and ^{13}C NMR (b) spectrum of 5,5'-bis(4-decylphenyl)-2,2'-bithiophene (DD-PTTP).

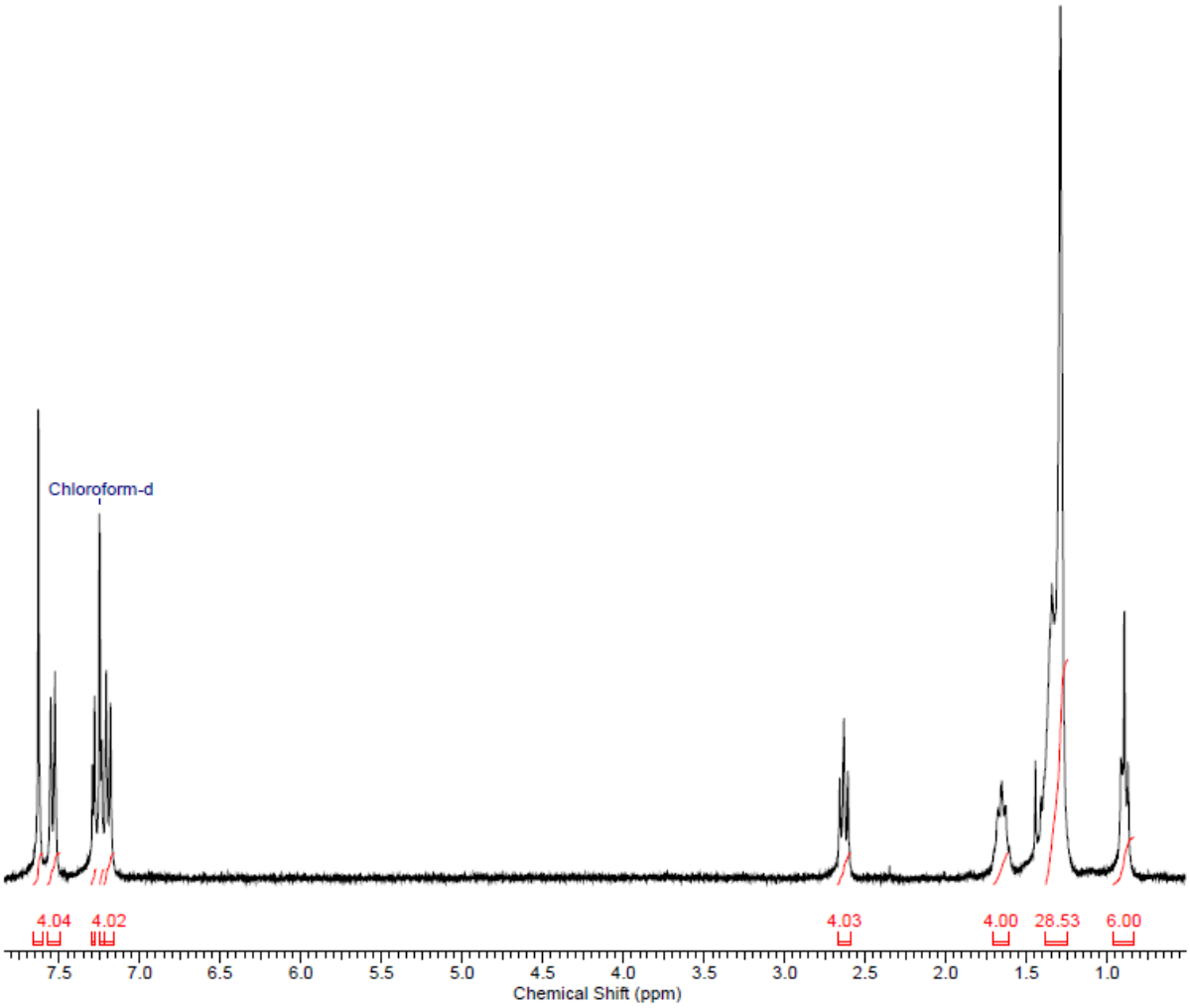

No.	Annotation	(ppm)
1	Chloroform-d	7.25

No.	(ppm)	Value	Absolute Value
1	[0.84 .. 0.96]	6.001	1.18325e+10
2	[1.25 .. 1.38]	28.526	5.62422e+10
3	[1.62 .. 1.71]	4.003	7.89269e+9
4	[2.59 .. 2.67]	4.032	7.94889e+9
5	[7.16 .. 7.22]	4.021	7.92766e+9
6	[7.22 .. 7.25]	1.967	3.87882e+9
7	[7.27 .. 7.30]	1.987	3.91815e+9
8	[7.50 .. 7.57]	4.043	7.97144e+9
9	[7.60 .. 7.66]	4.000	7.88649e+9

Figure S5. ^{1}H NMR spectrum of 5,5'-bis(4-decylphenyl)-2,2'-bithiophene (DD-PTPTP).

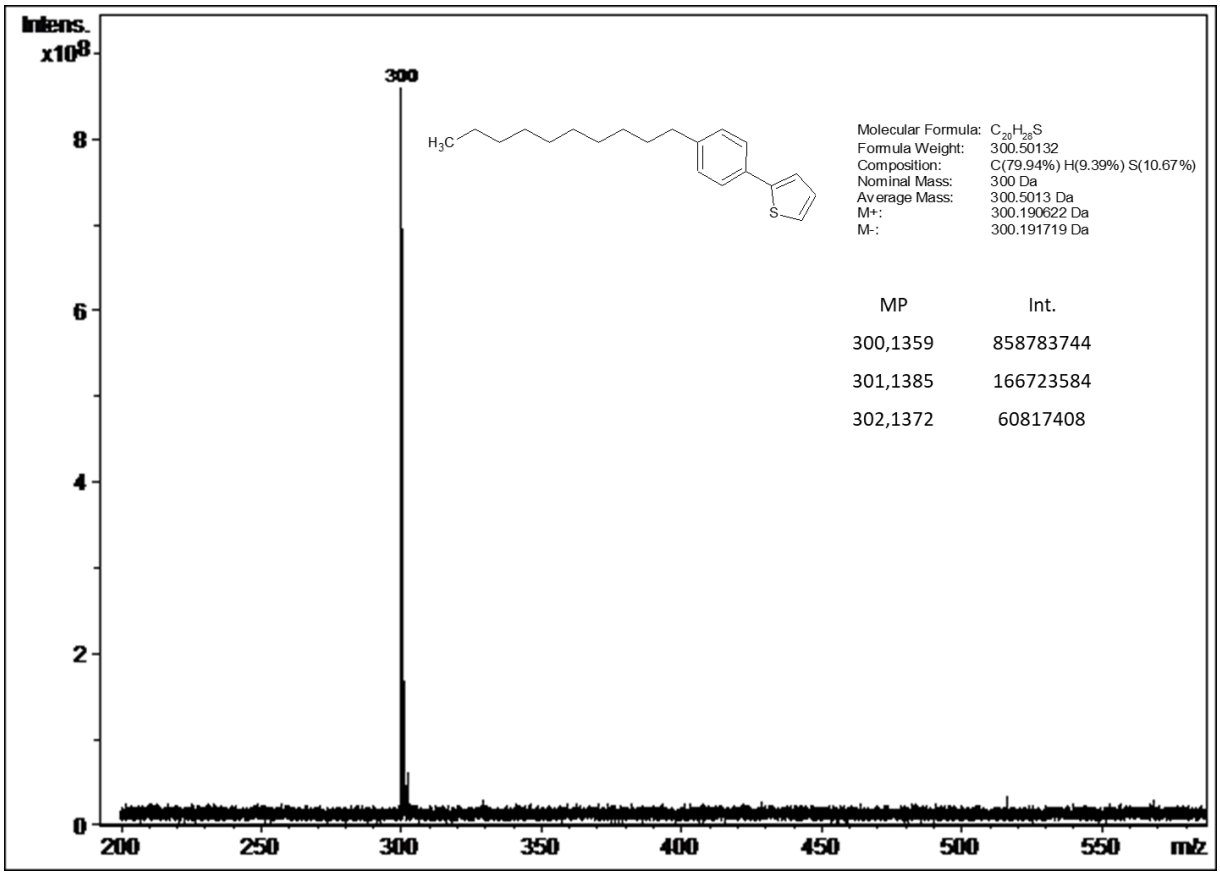

Figure S6. Mass spectrum of 2-(4-decylphenyl)thiophene (D-PT).

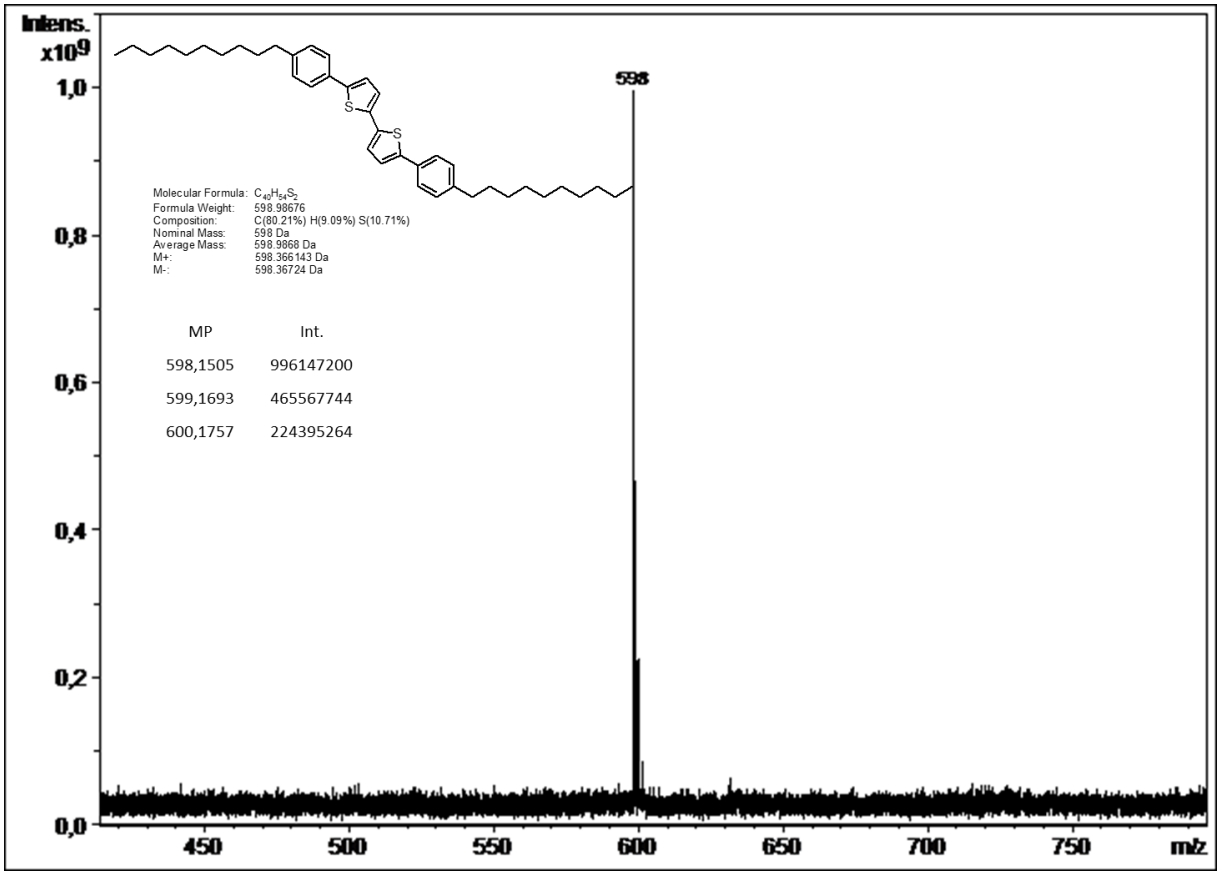

Figure S7. Mass spectrum of 5,5'-bis(4-decylphenyl)-2,2'-bithiophene (DD-PTTP).

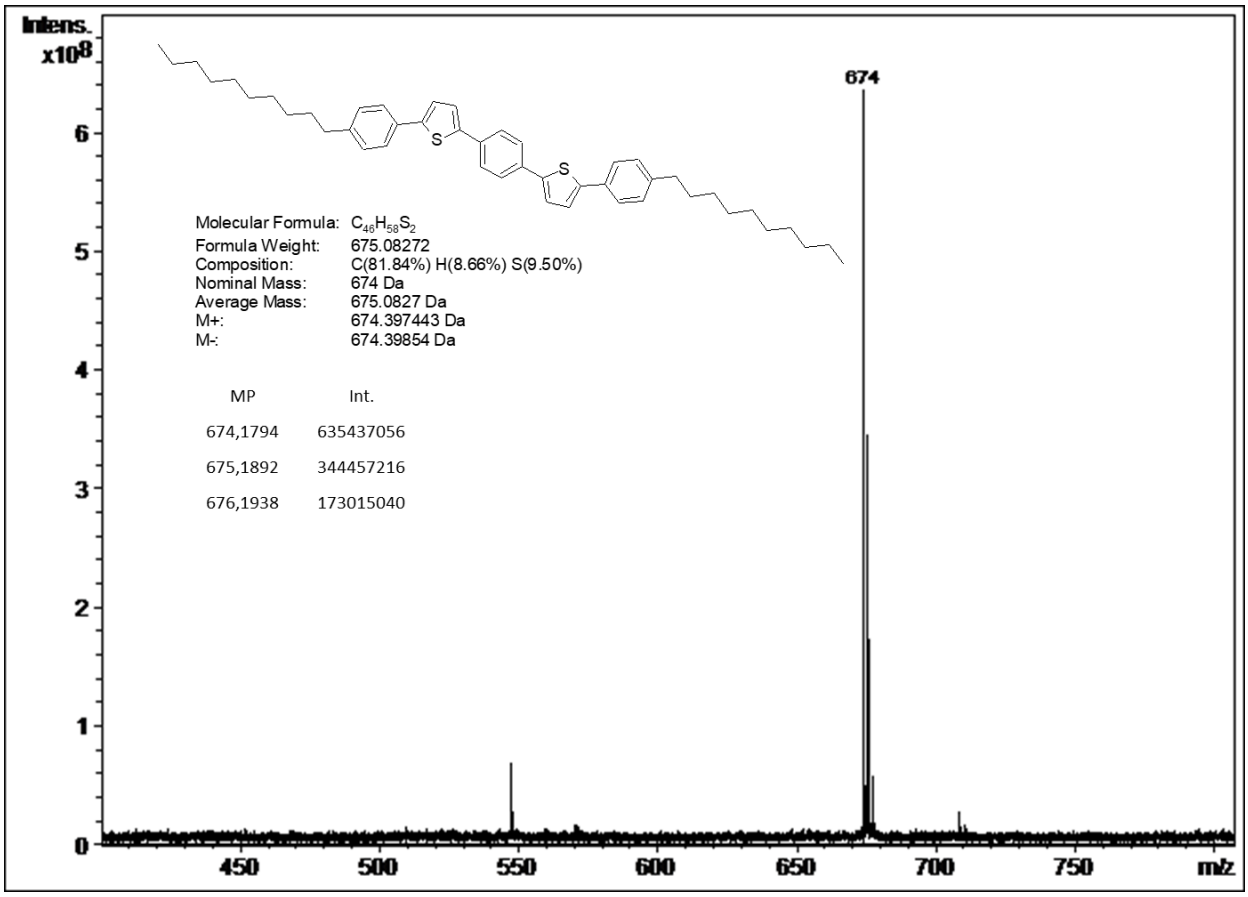

Figure S8. Mass spectrum of 2,2'-(1,4-phenylene)bis[5-(4-decylphenyl)thiophene] (DD-PTPTP).

3. Thermal analysis

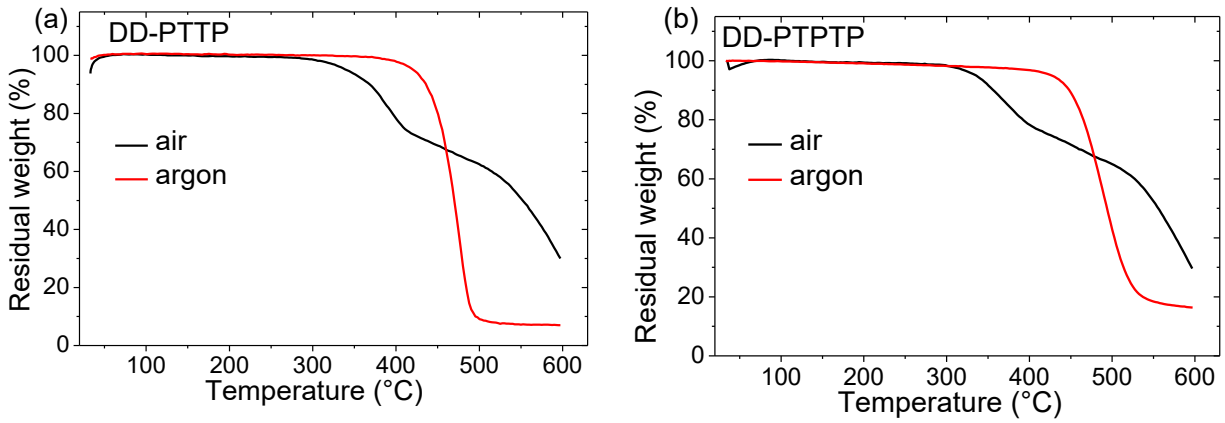

Figure S9. TGA data for DD-PTTP (a) and DD-PTPTP (b) polycrystalline powder.

Table S2. Suggested phase transitions in DD-PTTP and DD-PTPTP from the XRD (see the next section) and DSC data with the corresponding thermodynamic parameters at the phase transitions: the molar enthalpy change, ΔH, and the entropy changes, $\Delta S=\Delta H/T$, where T is the absolute temperature.

Oligomer	Phase transition	T [°C /K]	ΔH [kJ mol^{-1}]	ΔS [J K^{-1} mol^{-1}]
DD-PTTP	CrI → CrII	112/385	20	52
	CrII → I	211/484	37	77
DD-PTPTP	CrI → CrII	72/345	2.5	7.2
	CrII → SmC	248/521	33	63
	SmC → I	293/566	10	18

4. XRD and XRR data

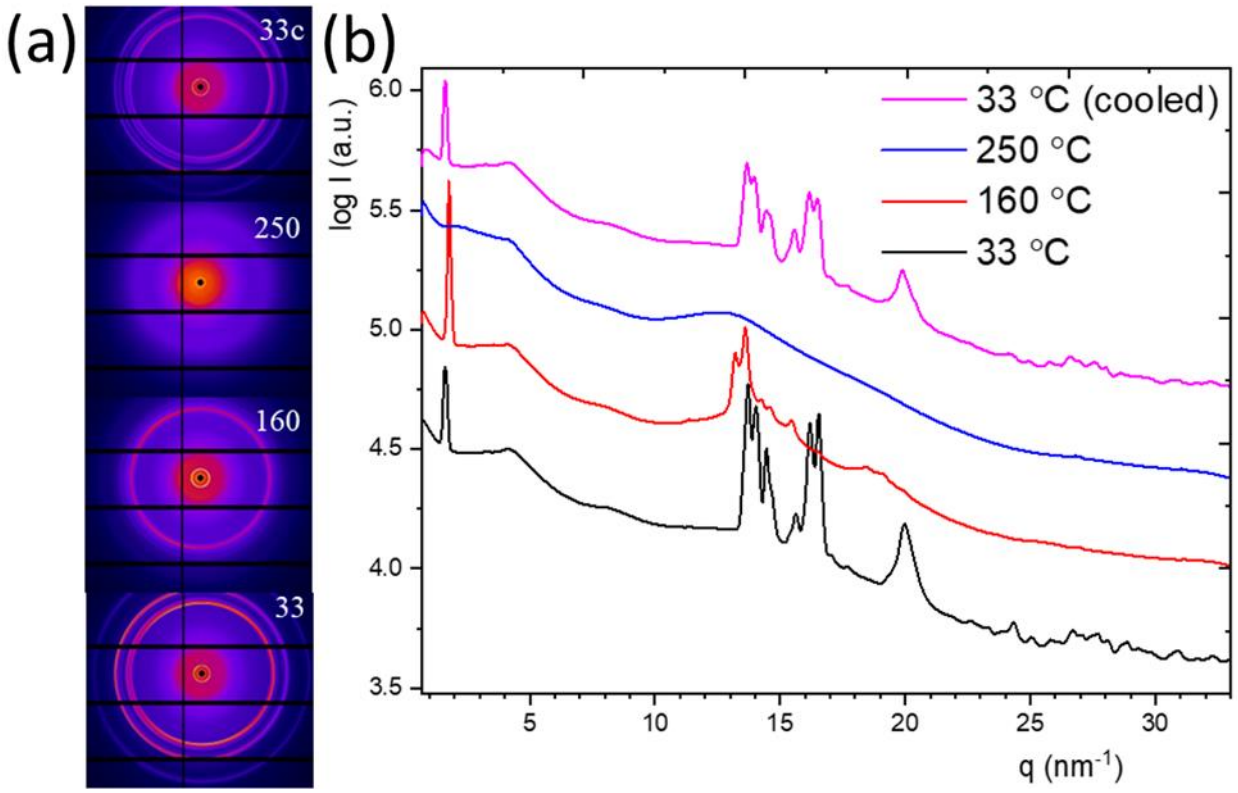

Figure S10. 2D XRD images (a) and the corresponding scans (b) recorded upon heating DD-PTTP and after its cooling. The scans are presented in the logarithmic scale and shifted vertically.

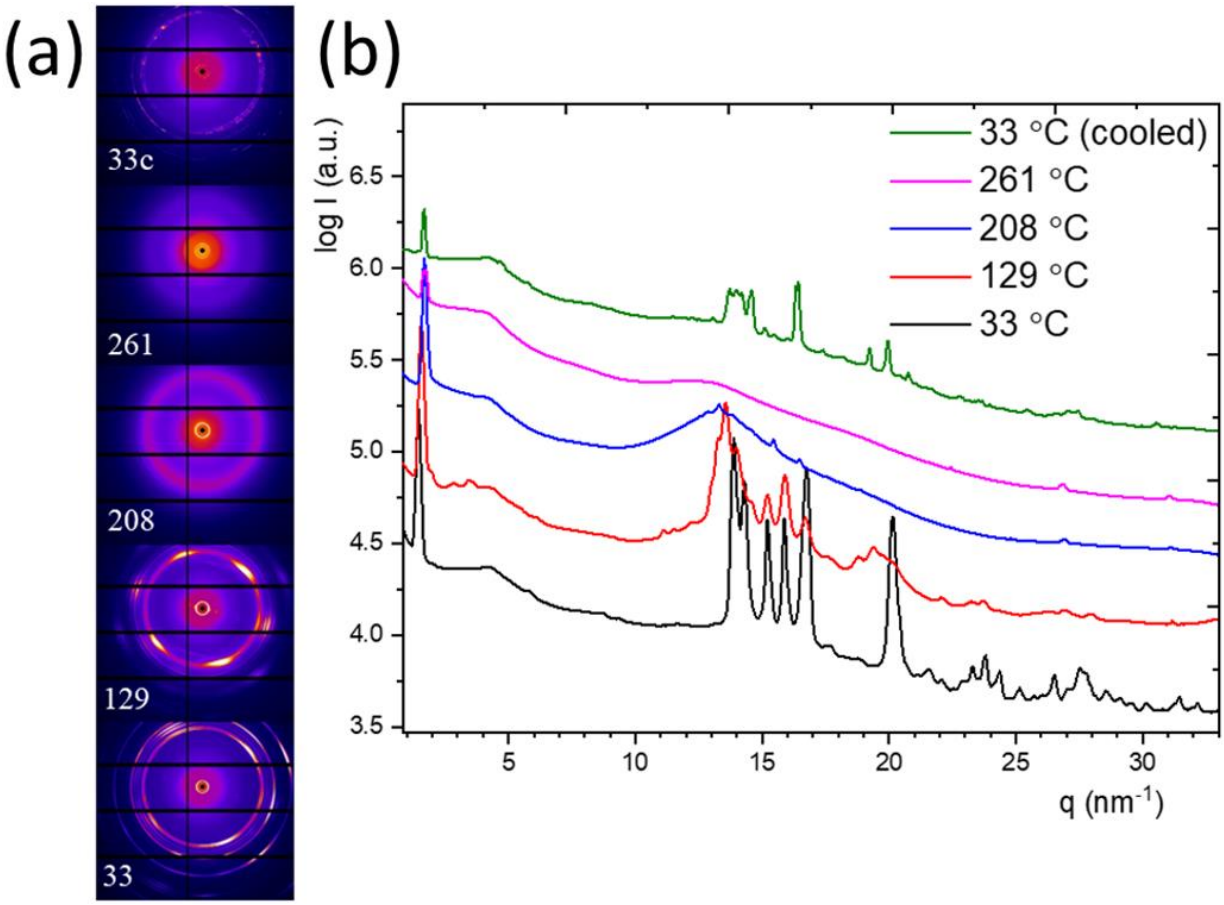

Figure S11. 2D XRD images (a) and the corresponding scans (b) upon heating DD-PTPTP and after its cooling. The scans are presented in the logarithmic scale and shifted vertically.

Table S3. Crystal parameters (orthorhombic lattice, P222) calculated from the XRD data for as-received and heated DD-PTTP and DD-PTPTP samples.

Sample	Temperature [°C]	*a* [nm]	*b* [nm]	*c* [nm]	*V* [nm^3]
DD-PTTP	33	3.88	1.641	0.381	2.426
DD-PTTP	160	3.458	0.924	0.478	1.527
DD-PTPTP	33	4.313	0.429	0.915	1.693
DD-PTPTP	129	3.997	3.209	0.566	7.260

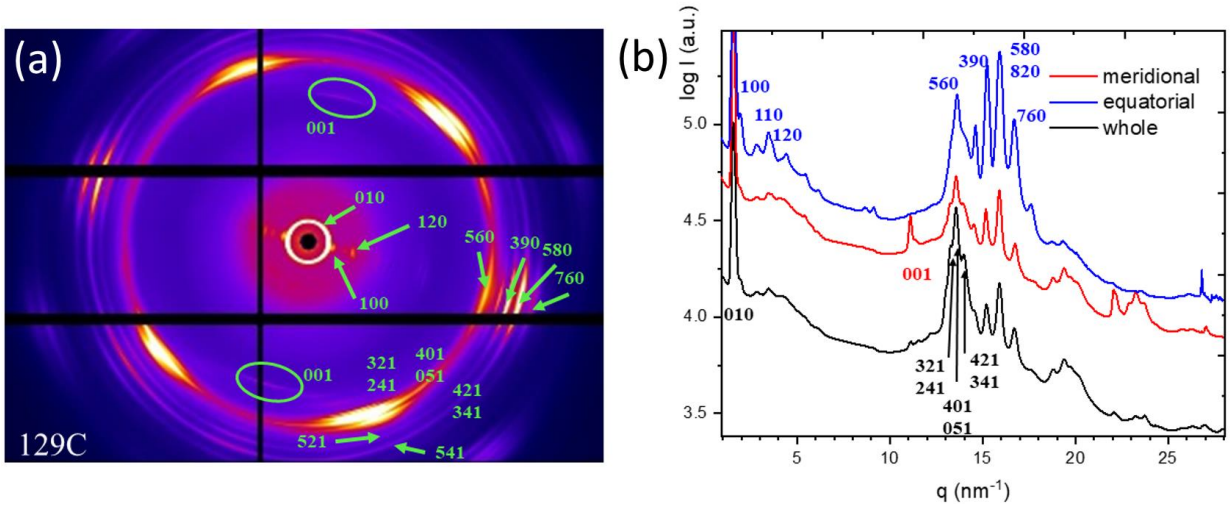

Figure S12. Indexed XRD data for DD-PTPTP recorded at 129 °C (from Figure S11) and the corresponding equatorial, meridional, and whole scans.

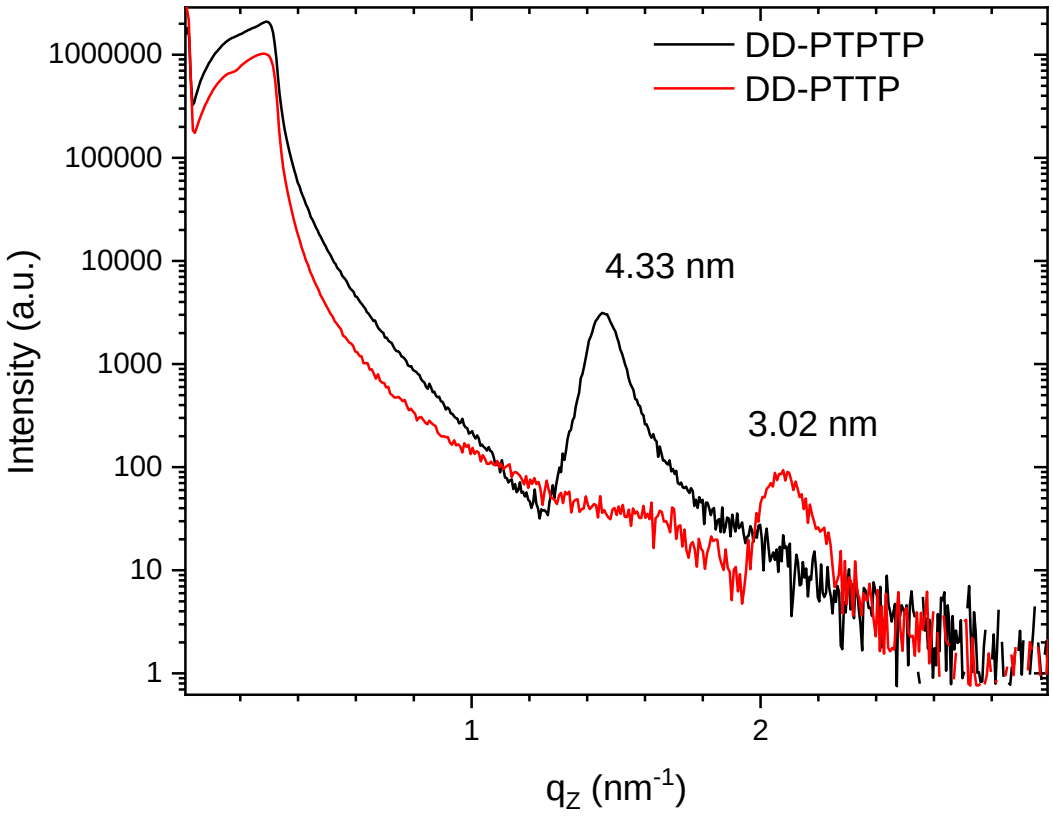

Figure S13. XRR curves for thermally evaporated thin films of DD-PTTP and DD-PTPTP (the detailed of film preparation are given in Section 2.6 of the main text). The observed Bragg reflections are marked with the corresponding *d*-spacings, which are attributed to the thickness of the molecular layers.

5. Optical microscopy data

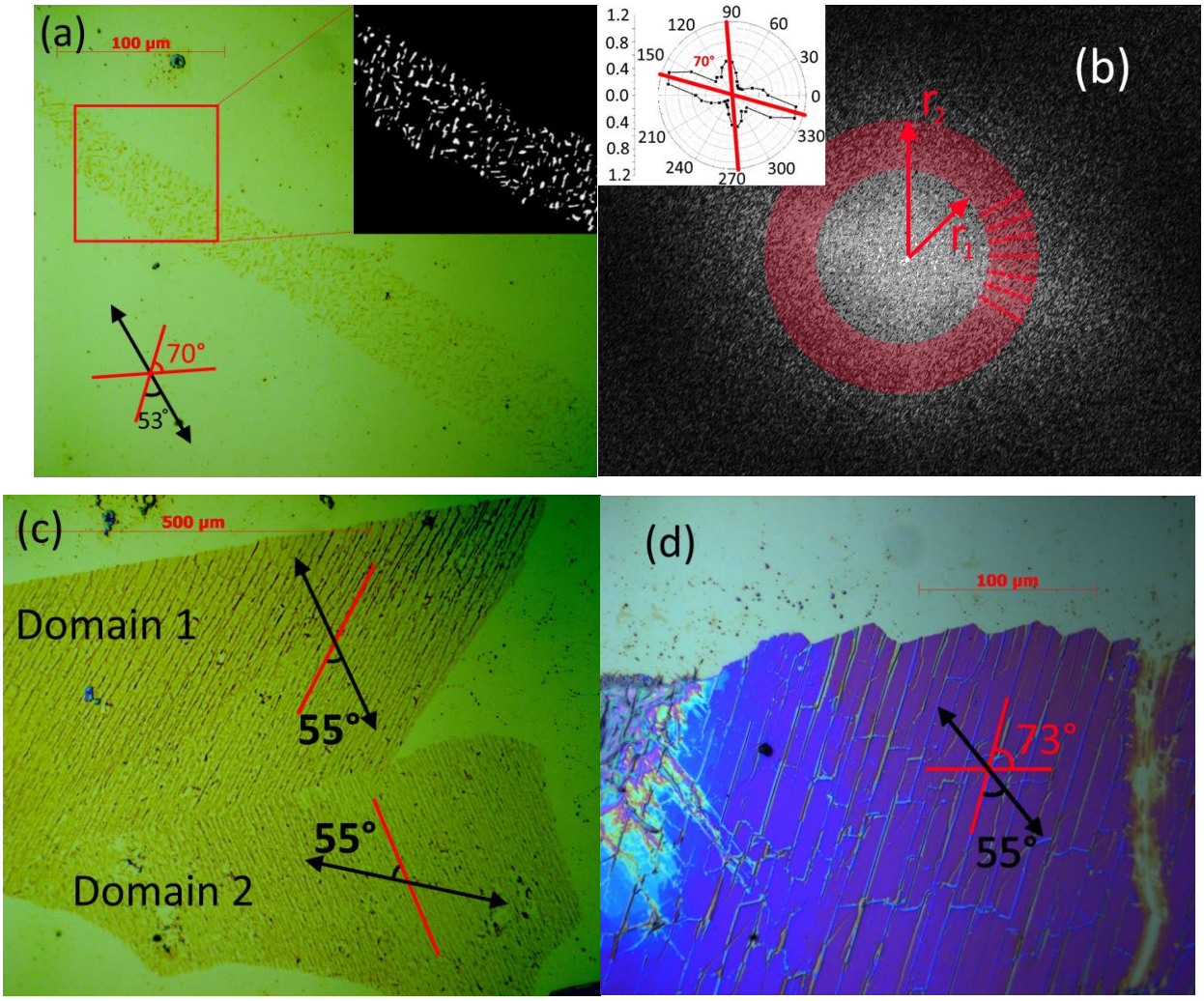

Figure S14. Optical images of annealed DD-PTTP crystals of different thicknesses: monolayer (a), few-layers (c), and 3D (d) films. Red lines on panel (a) represent two primary directions of dewetted pattern, black arrow represents the PL polarization direction, the inset shows a black-and-white image with enhanced contrast of the area marked by the red rectangle. Panel (b) represents the modulus of fast-Fourier transform of the image presented in the inset of panel (a). Inset in panel (b) shows circular diagram obtained by integration over segments marked by dashed red lines within the semi-transparent red ring, from r_1 to r_2. Black arrows on panels (c) and (d) represent polarization maxima of PL from the corresponding domains, and red lines represent orientations of the annealing-induced patterns.

The image of a thermally treated DD-PTTP monolayer film, shown in the inset on panel (a), was processed as following. First, surrounding impurities and noise were removed from the image. Second, a background plane of 2nd order was subtracted from the image, and the contrast of the inverted image (by colour) was maximized by the threshold of 0.3 from the average monolayer height, resulting in the monochrome black background and white island-like structures on it. Then,

the image was processed by 2D fast Fourier transform. Profiles from this image were extracted along lines passing through the center of the image at different angles and were averaged over a 15-pixel wide stripe along the lines. The obtained profiles were smoothed, and their widths at half-height were calculated. After that, the baseline of the angular plot was subtracted, and result was plotted as shown on the inset of Figure S14b.

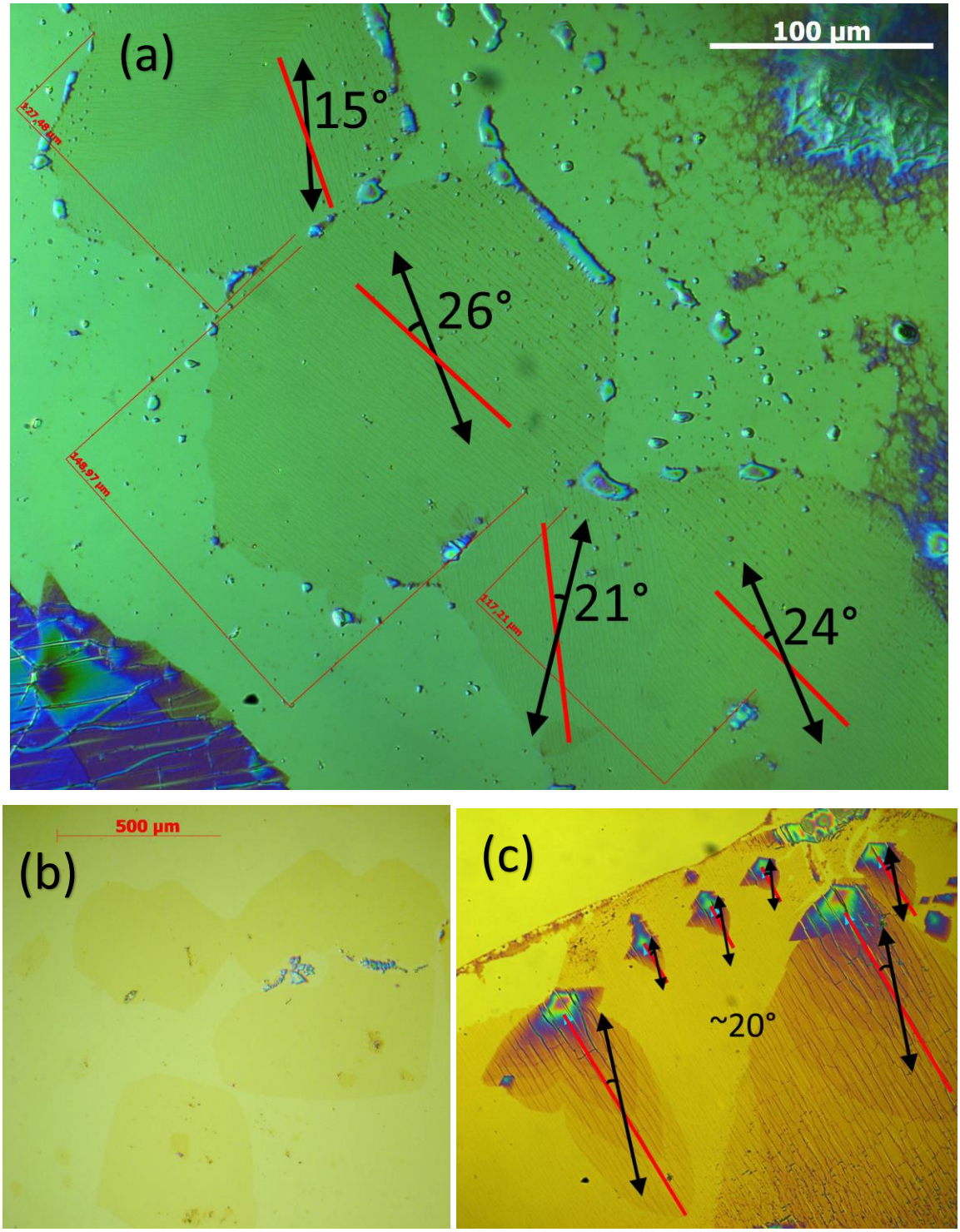

Figure S15. Optical (C-DIC) images of DD-PTPTP crystals: annealed monolayer (a), neat monolayer (b), and annealed thicker crystals (c). Black arrows show directions of PL polarization. Red lines represent directions of elongated patterns.

6. Optical spectroscopy data

6.1. Solutions

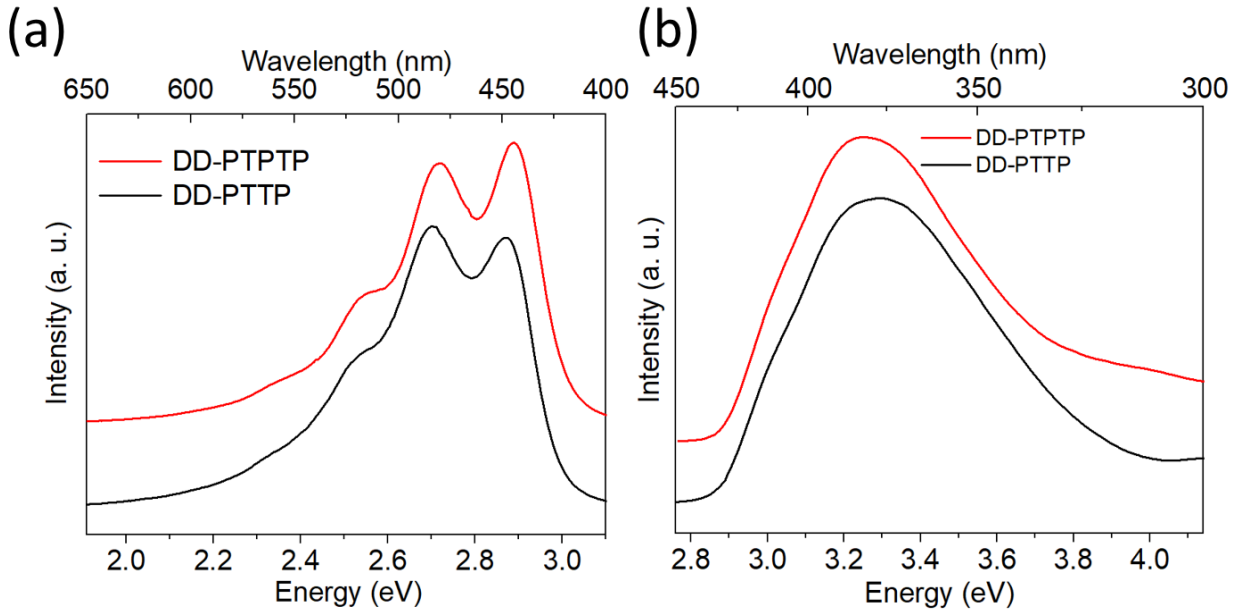

Figure S16. PL (a) and absorption (b) spectra of DD-PTTP and DD-PTPTP in THF solution. The oscillator strengths calculated from their absorption spectra according to Eq. (4) in Ref.[1] were 0.88 for DD-PTTP and 1.4 for DD-PTPTP.

The PL quantum yield, Φ, can be determined via the radiative, k_r, and nonradiative, k_{nr}, rate constants as

$$\Phi = \frac{k_r}{k_r + k_{nr}} . \qquad (1)$$

The k_r values calculated according to Eq. (9b) in Ref.[1] from the Φ values and the oscillator strengths, and the absorption/PL spectra (Figure S16) were 0.45 ns^{-1} for DD-PTTP and 0.72 ns^{-1} for DD-PTPTP. The k_r values calculated from Eq. (1) with the use of the k_r+k_{nr} values measured from the fluorescence lifetimes in THF solution for TMS-PTTP-TMS[2] and TMS-PTPTP-TMS,[3] where TMS stands for trimethylsilyl, were 0.55 ns^{-1} for DD-PTTP and 0.77 ns^{-1} for DD-PTPTP. Accordingly, the k_r values calculated from the steady-state optical data and from the fluorescence lifetimes are in very good correspondence for both oligomers.

Following the Strickler-Berg equation,[1,4] if the absorption and PL spectra have the identical shapes and positions, the ratio of the radiative rates in DD-PTPTP and DD-PTTP in the same solvent is

$$\frac{k_r(PTPTP)}{k_r(PTTP)} = \frac{f(PTPTP)}{f(PTTP)} = \frac{\varepsilon(PTPTP)}{\varepsilon(PTTP)} = \frac{60 \times 10^3}{39 \times 10^3} = 1.54, \qquad (2)$$

where f is the oscillator strength of the $S_0 \rightarrow S_1$ transition, and ε is the molar extinction. Therefore, combining Eqs. (1) and (2), we obtain the ratio of k_{nr} for the two oligomers:

$$\frac{k_{nr}(PTPTP)}{k_{nr}(PTTP)} = \frac{k_r(PTPTP)(\Phi^{-1}(PTPTP) - 1)}{k_r(PTTP)(\Phi^{-1}(PTTP) - 1)} = 0.089 \approx \frac{1}{11}. \quad (3)$$

Note that DDs in Eqs. (2) and (3) are omitted for brevity.

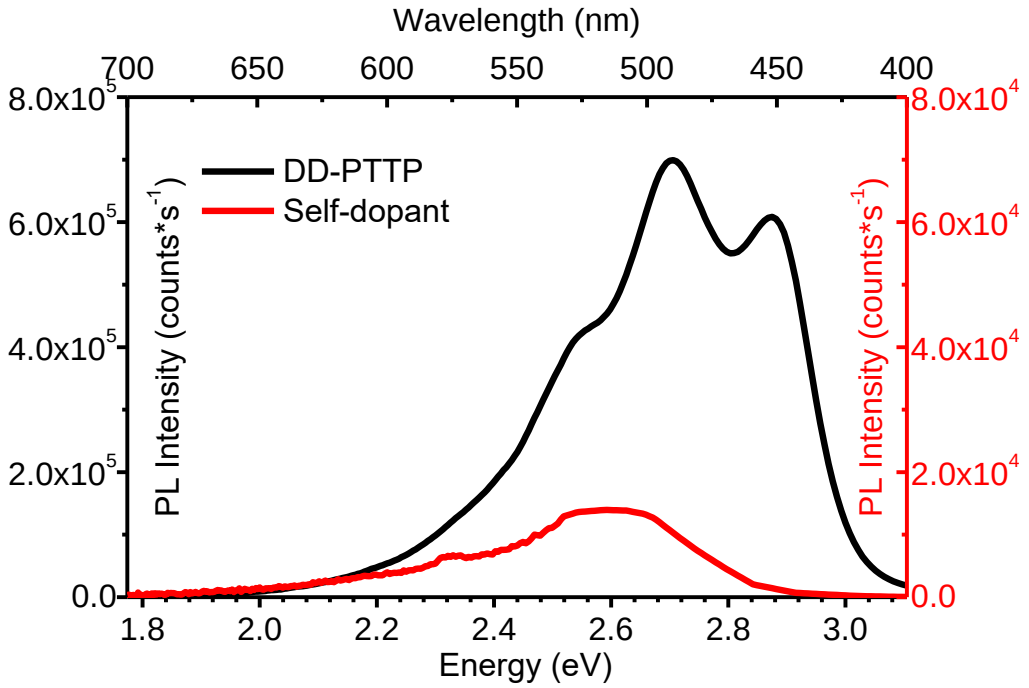

Figure S17. PL spectra of DD-PTTP and its self-dopant in THF solutions recorded at excitation wavelengths of 378 and 460 nm, respectively. The PL excitation band is subtracted from the self-dopant spectrum. The suggested molecular structure of the self-dopant is DD-P4TP according to the studies presented in Ref. [5], and this is confirmed by the position of the self-dopant PL spectrum, which is nearly the same as that of TMS-P4TP-TMS (the self-dopant for TMS-PTTP-TMS). The molar self-doping level 0.002% (20 ppm) was evaluated assuming that the molar extinction and the PL quantum yield of the self-dopant equal to those of TMS-P4TP-TMS,[5] that is the impact of the non-conjugated terminal substituents on the PL data is suggested to be negligible.

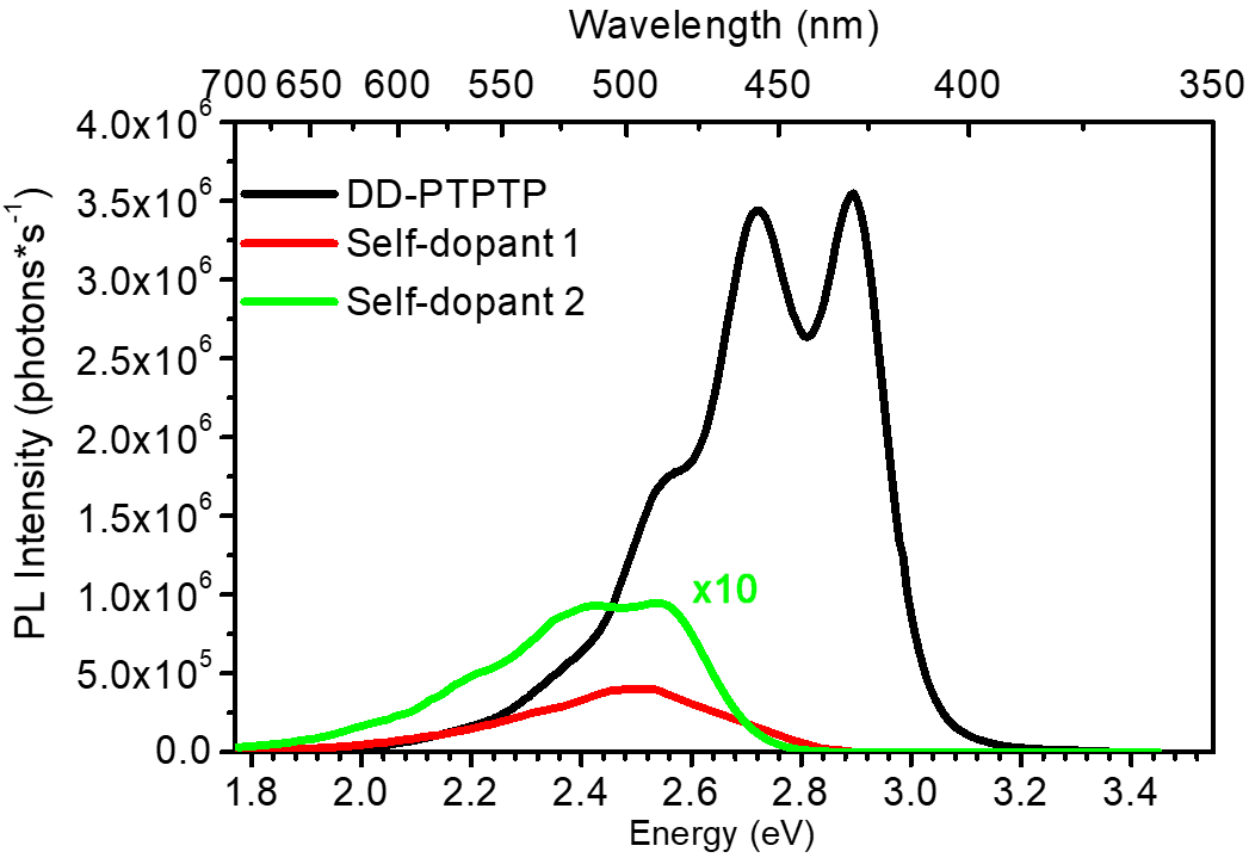

Figure S18. PL spectra of DD-PTPTP and its self-dopant THF solutions recorded at excitation wavelengths of 382 and 460 nm, respectively. The PL excitation band is subtracted from the self-dopant spectra. As the molecular structure of the self-dopant is unknown, to estimate the self-doping ratio, the molar extinction and the PL quantum yield of the self-dopant are assumed to be equal to those of DD-PTPTP. As a result, the molar self-doping ratio of 0.03% (300 ppm) was estimated for the high-vacuum purified sample (green line). To record the self-dopant PL spectrum with high signal-to-noise ratio, a sample prior high-vacuum purification was used (red line).

6.2. 2D crystals

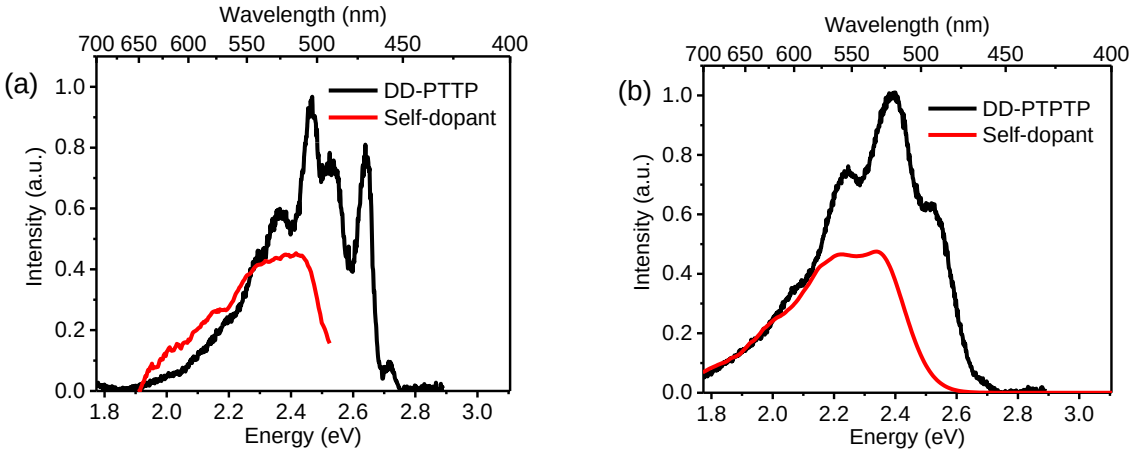

Figure S19. PL spectra of DD-PTTP (a) and DD-PTPTP (b) 2D crystals (black) and self-dopants (red). The corresponding self-dopants spectra are taken from Figure S17 and Figure S18 and then red shifted by 0.2 eV (this shift corresponds to the solid-state shift for DD-PTTP and DD-PTPTP as described in the main text).

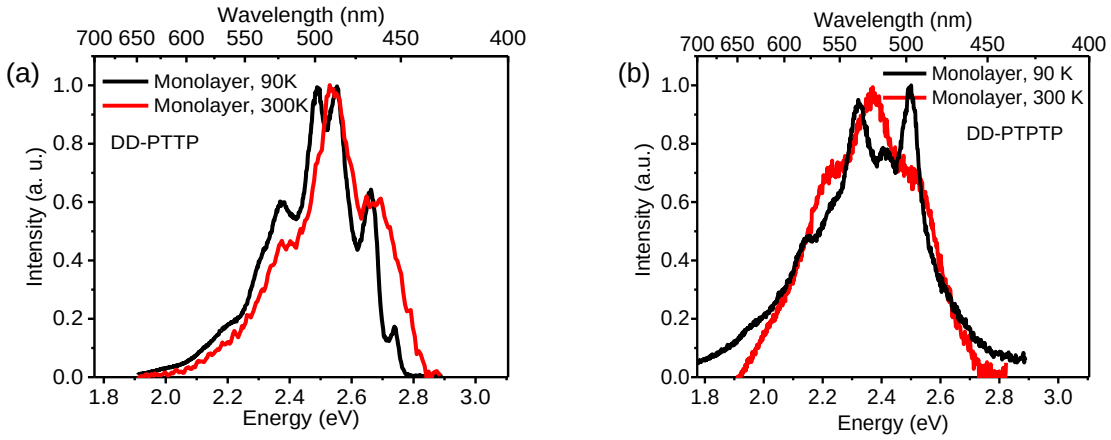

Figure S20. PL spectra of DD-PTTP (a) and DD-PTPTP (b) monolayers recorded at 90 K and 300 K.

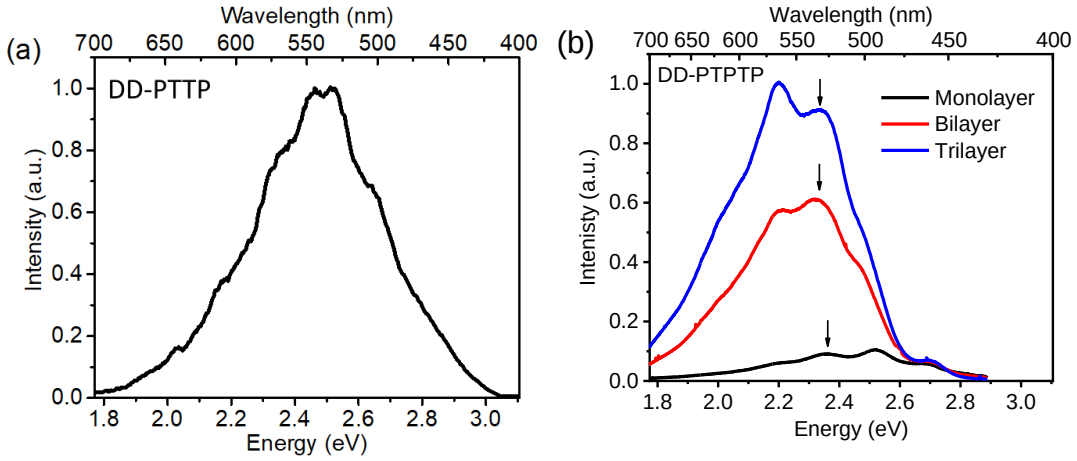

Figure S21. Room-temperature PL spectra of a few-layers DD-PTTP crystal (a) and DD-PTPTP crystals of different thicknesses (b). Arrows in panel (b) mark the self-dopant 00 transition, whose red shift in the bilayer and trilayer crystals can be explained by the more polarizable dielectric environment of luminophores as compared with that of the monolayer.

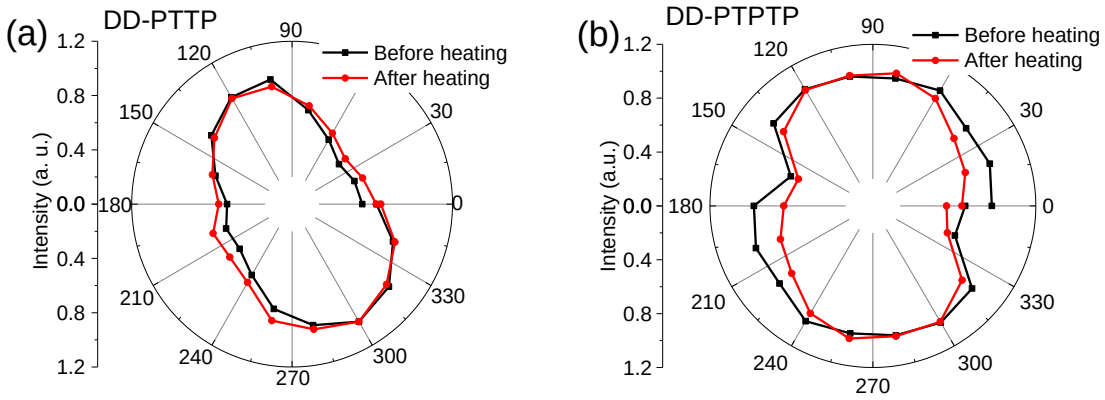

Figure S22. PL polarization diagram of DD-PTTP (a) and DD-PTPTP (b) monolayer sample before (black) and after (red) annealing (see the details in the main text). Zero angle (0°) marks the polarization of excitation radiation.

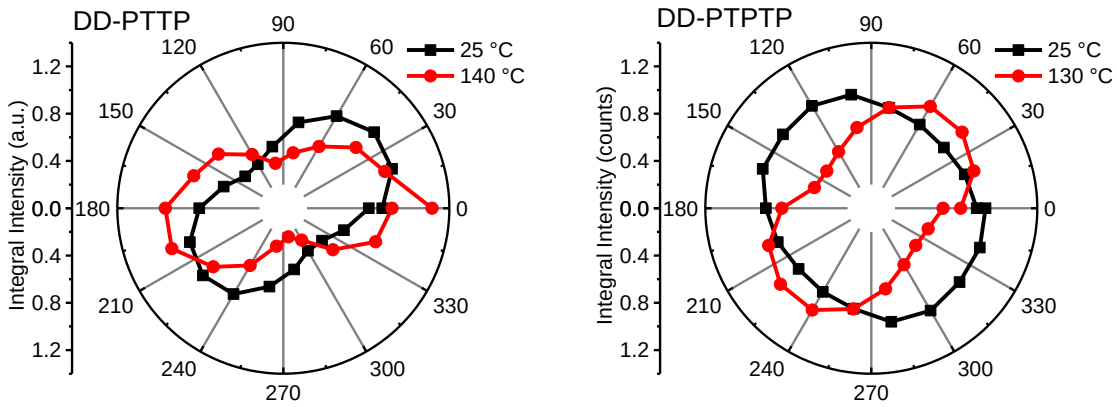

Figure S23. PL polarization diagrams of a few layers DD-PTTP (a) and DD-PTPTP (b) crystals recorded at 25 °C (CrI) and temperatures above the CrI→CrII phase transition (see Figure 3 for the DSC data). To decrease the sample degradation, the PL polarization diagrams were recorded as averages over series of PL spectra captured within a map (~100 different spots on the sample with interspot spacing of ~10 μm) at various polarizer orientations. Zero angle (0°) marks the polarization of excitation radiation. The PL spectra were averaged over the map and integrated over 450–600 nm. For each material, the orientation of the diagram maximum and its axis ratio change, which can be assigned to reorientation of the dipole transition moments of the molecules in the crystal unit cell upon the CrI→CrII phase transition as was observed earlier for other 2D crystals (Ref.12 in the main text).

6.3. Discussion of the L and H sub-bands in the PL spectra of 2D DD-PTTP crystals

We argue here that the L and H sub-bands observed in 2D DD-PTTP crystals at 90 K (Fig. 8a) are not associated with the Davydov splitting.[6] First, as the splitting of 0.07±0.01 eV is about one order of magnitude higher than the thermal energy (kT=0.008 eV, where k is the Boltzmann constant, and T=90 K is the temperature), the intensity of the higher energy Davydov state should be much less than that of the lower energy state. However, the intensities of the L and H sub-bands are comparable (Fig. 8a). Second, the 00 states in the upper and lower Davydov bands should have mutually orthogonal polarizations,[6] whereas both sub-bands show the very similar orientations of the polarization diagrams (Figure S24).

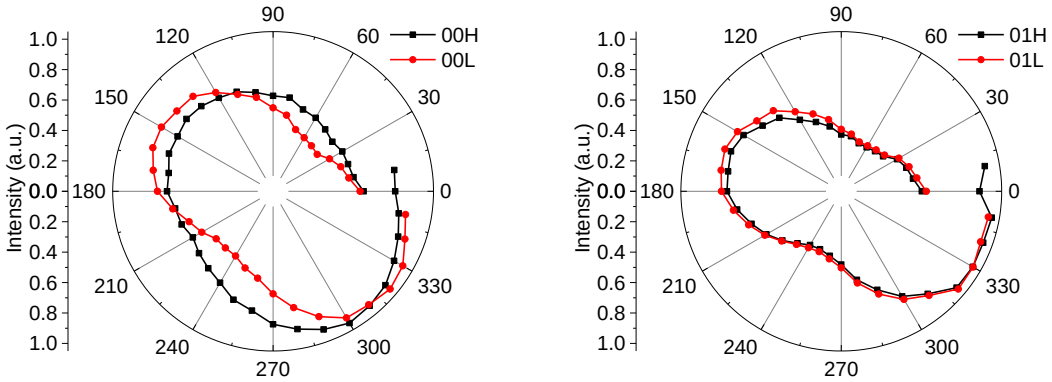

Figure S24. PL polarization diagrams for the L and H sub-bands in the 00 (left) and 01 (right) bands of a few-layers DD-PTTP crystal at 90 K. The PL polarization diagrams were recorded clockwise, and they are not closed because of sample degradation resulting in a decrease in the PL intensity. Zero angle (0°) marks the polarization of excitation radiation.

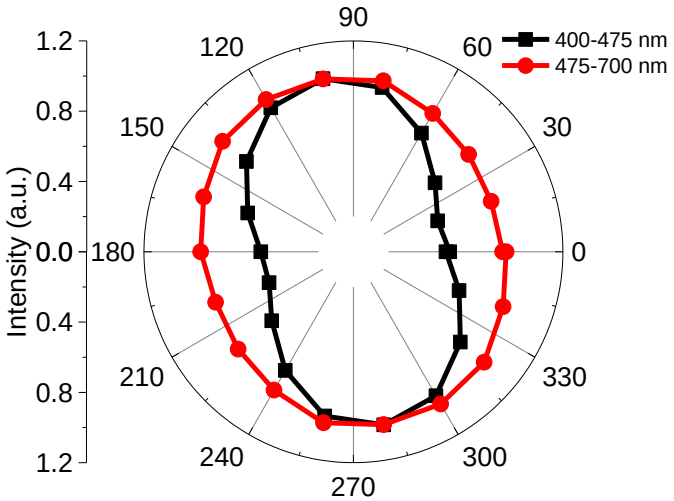

Figure S25. Polarization diagrams for a few-layers DD-PTPTP crystal recorded at room temperature. Black and red curves correspond to the integrals over the spectral ranges 400–475 nm and 475–700 nm, respectively. The different aspect ratio of these polarization diagrams signifies that they correspond to different luminophores assigned to DD-PTPTP and its self-dopant. Zero angle (0°) marks the polarization of excitation radiation.

7. 2D OFETs

Table S4. OFETs characteristics.

Sample number	W/L	$V_{th(sat)}$ [V]	$V_{th(lin)}$ [V]	μ_{lin} [cm^2/Vs]	μ_{sat} [cm^2/Vs]	r_{lin}^f [%]
Monolayer OFETs based on DD-PTTP						
1	4.7±0.3	–4.1	–6.5	0.17±0.01	0.14±0.01	71
2	4.0±0.3	–4.6	–8.0	0.15±0.01	0.14±0.01	68
3	2.7±0.3	–6.8	–5.8	0.15±0.02	0.13±0.02	75
4	2.6±0.2	–3.1	–7.2	0.11±0.01	0.09±0.001	70
5	5.1±0.3	–4.1	–5.9	0.14±0.01	0.13±0.01	71
6	1.8±0.2	–6.0	–7.9	0.13±0.02	0.13±002	67
Average± standard deviation		–4.8±1.4	–6.9±1.0	0.14±0.02	0.12±0.02	
Best				0.17±0.01	0.14±0.01	
Few-layers OFETs based on DD-PTTP						
1	0.82±0.14	–14.2	–5.4	0.11±0.02	0.11±0.02	61
2	0.71±0.09	–14.4	–12.8	0.09±0.01	0.09±0.01	60
3	1.12±0.12	–7.3	–8.7	0.11±0.01	0.12±0.01	69
4	0.68±0.09	–30.1	–29.3	0.12±0.01	0.12±0.01	51

Average± standard deviation		–17±10	–14±11	0.11±0.02	0.11±0.02	
Best				0.12±0.01	0.12±0.01	
Monolayer OFETs based DD-PTPTP						
1	1.4±0.1	–2.1	–1.5	0.15±0.01	0.17±0.01	83
2	3.5±0.3	–1.0	–2.2	0.19±0.02	0.20±0.02	90
3	2.2±0.2	2.6	1.3	0.21±0.02	0.21±0.02	94
4	1.8±0.2	2.5	2.6	0.20±0.02	0.23±0.02	95
5	2.7±0.3	3.5	4.4	0.15±0.01	0.17±0.01	91
6	1.4±0.2	2.8	2.6	0.15±0.02	0.14±0.02	93
Average± standard deviation		1.4±2.3	1.2±2.6	0.18±0.03	0.19±0.03	
Best				0.21±0.02	0.23±0.02	
Few-layers OFETs DD-PTPTP						
1	4.2±0.3	0.5	1.0	0.18±0.02	0.12±0.01	84
2	4.1±0.3	–0.1	0.1	0.19±0.02	0.14±0.01	85
3	2.2±0.3	1.4	0.8	0.15±0.02	0.15±0.02	85
4	2.1±0.2	4.0	3.2	0.15±0.02	0.15±0.02	94
5	2.2±0.3	4.0	2.8	0.14±0.03	0.14±0.03	86
Average± standard deviation		2.5±1.8	1.6±1.3	0.16±0.02	0.14±0.01	
Best				0.19±0.02	0.15±0.02	

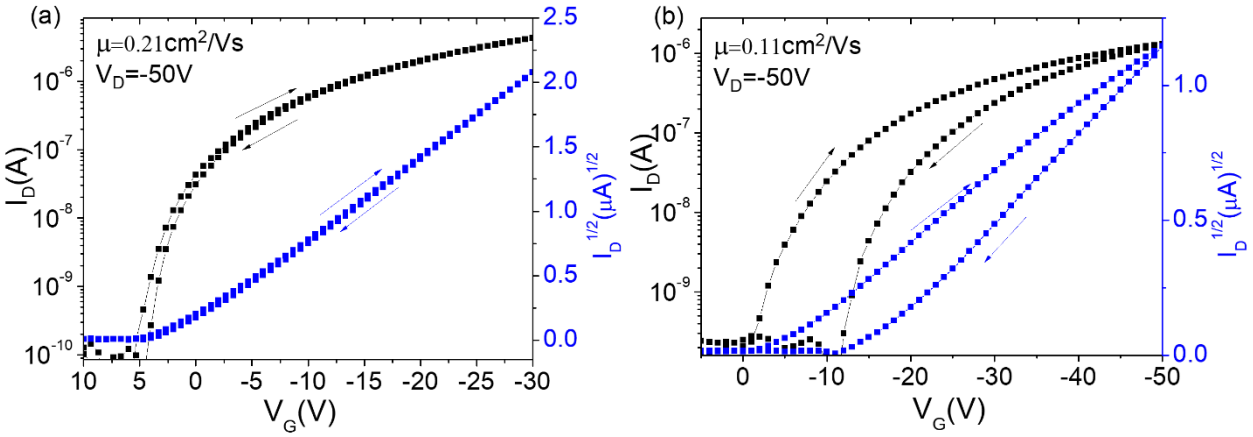

Figure S26. Transfer characteristics for monolayer (a) and few-layers (b) DD-PTTP OFETs in the saturation regime.

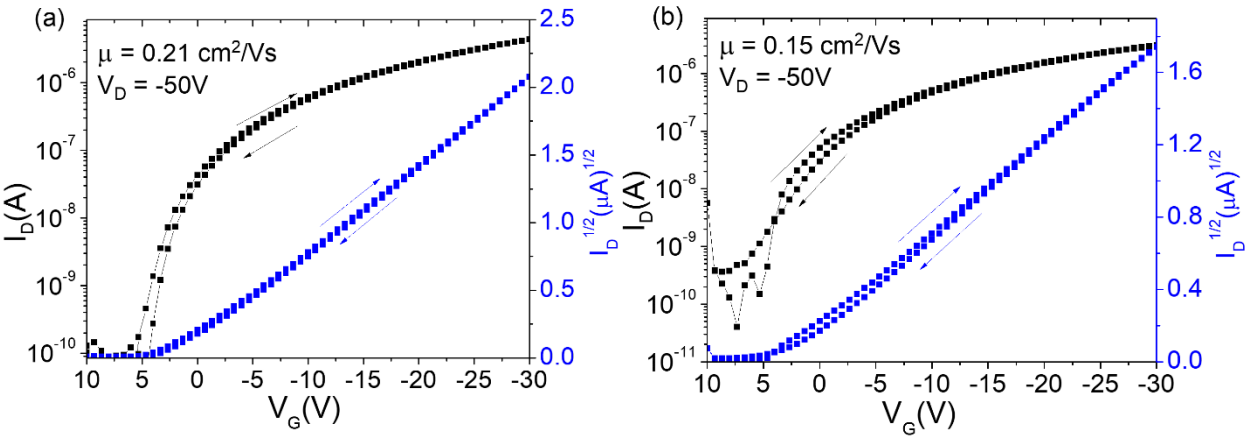

Figure S27. Transfer characteristics for monolayer (a) and few-layers (b) DD-PTPTP OFETs in the saturation regime.

8. OLETs

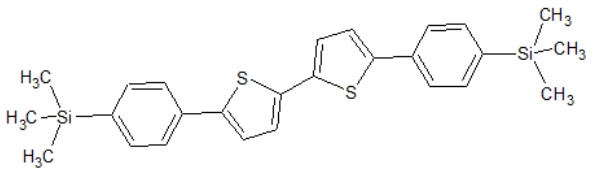

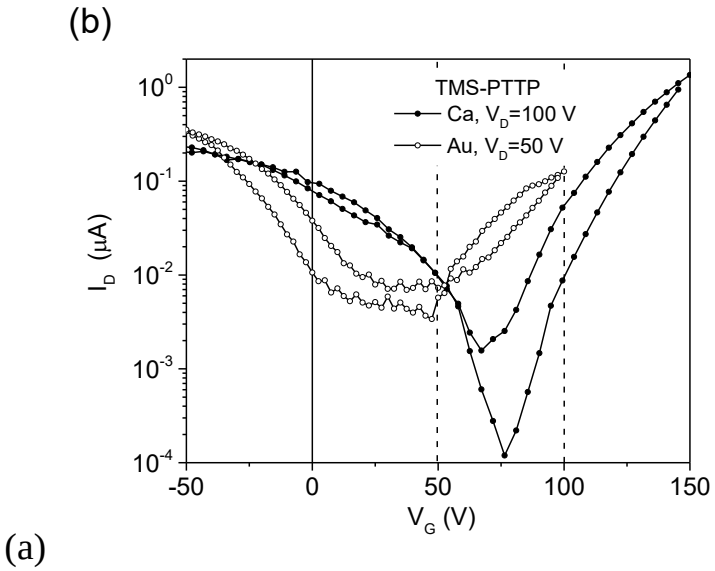

Figure S28. Structure of PTTP derivative with trimethylsilyl (TMS) terminal groups, TMS-PTTP (a), transfer characteristics of 3D SC TMS-PTTP OFETs with symmetric Ca and Au source/drain electrodes (b). The 3D TMS-PTTP single crystals were grown, as described in Ref.[2], then transferred and laminated onto Si/SiO_2 substrates covered with PMMA layer (its deposition details are given in Section 2.6); then Ca or Au electrodes were deposited on the top of TMS-PTTP crystals by thermal vacuum evaporation as described in Section 2.6; all stages of preparation and characterization were carried out in the inert atmosphere using gloveboxes. The transfer characteristics are V-shaped indicating the ambipolar charge transport for both type of electrodes.

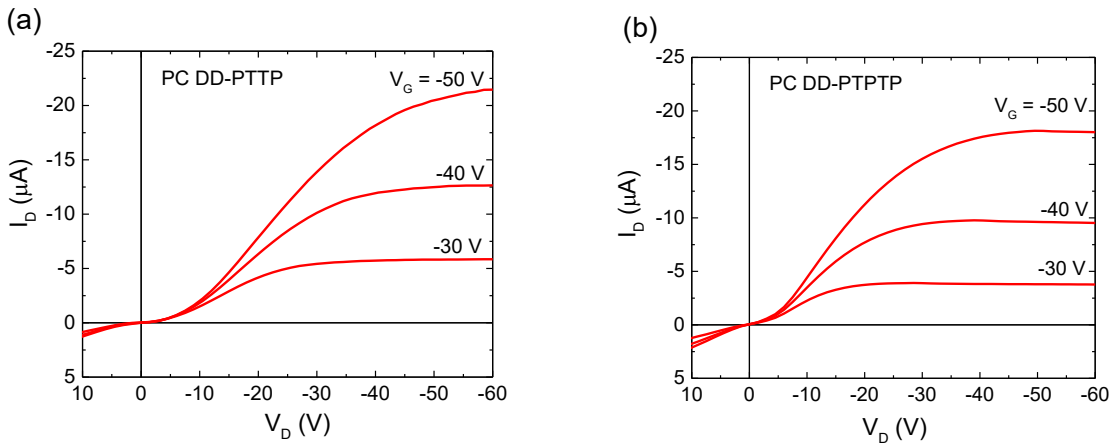

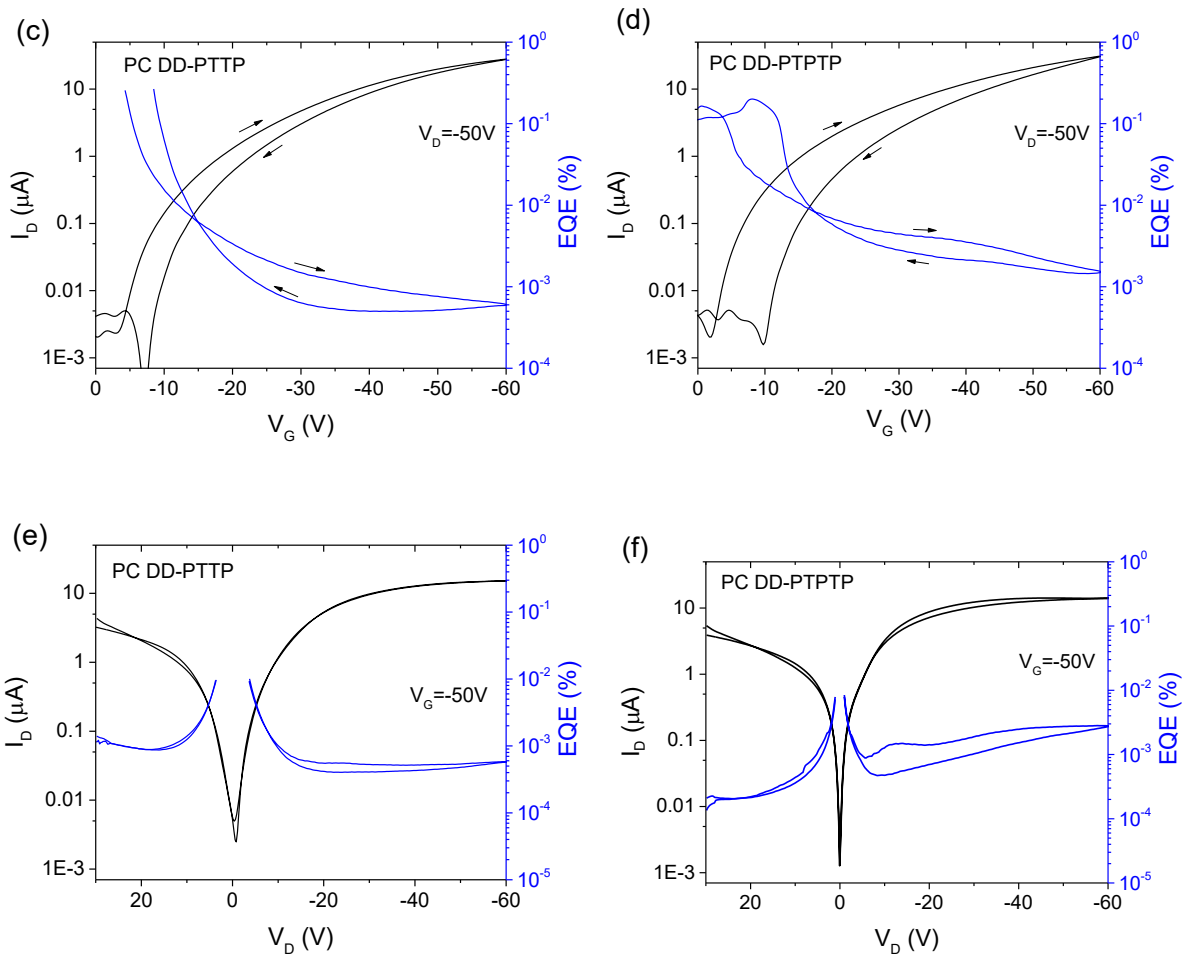

Figure S29. PC OLETs: output characteristics (a,b), EL EQE vs V_G dependences (c,d) and EL EQE vs V_D dependences (e,f) for DD-PTTP (a,c,e) and DD-PTPTP (b,d,f). Interestingly, the character of the EL EQE vs V_D dependence is different for two studied oligomers: for PC DD-PTTP, the EQE is almost constant in range of V_D from –10 to –60 V, while, for PC DD-PTPTP, the EL EQE increases about one order while V_D changes from –10 to –60 V.

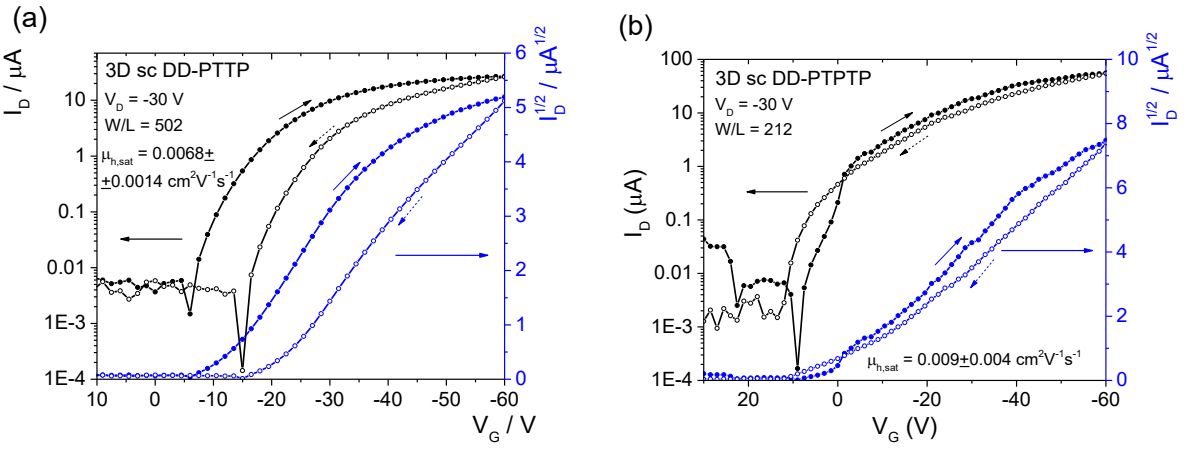

Figure S30. Typical transfer characteristics of 3D SC OLETs based on DD-PTTP (a) and DD-PTPTP (b).

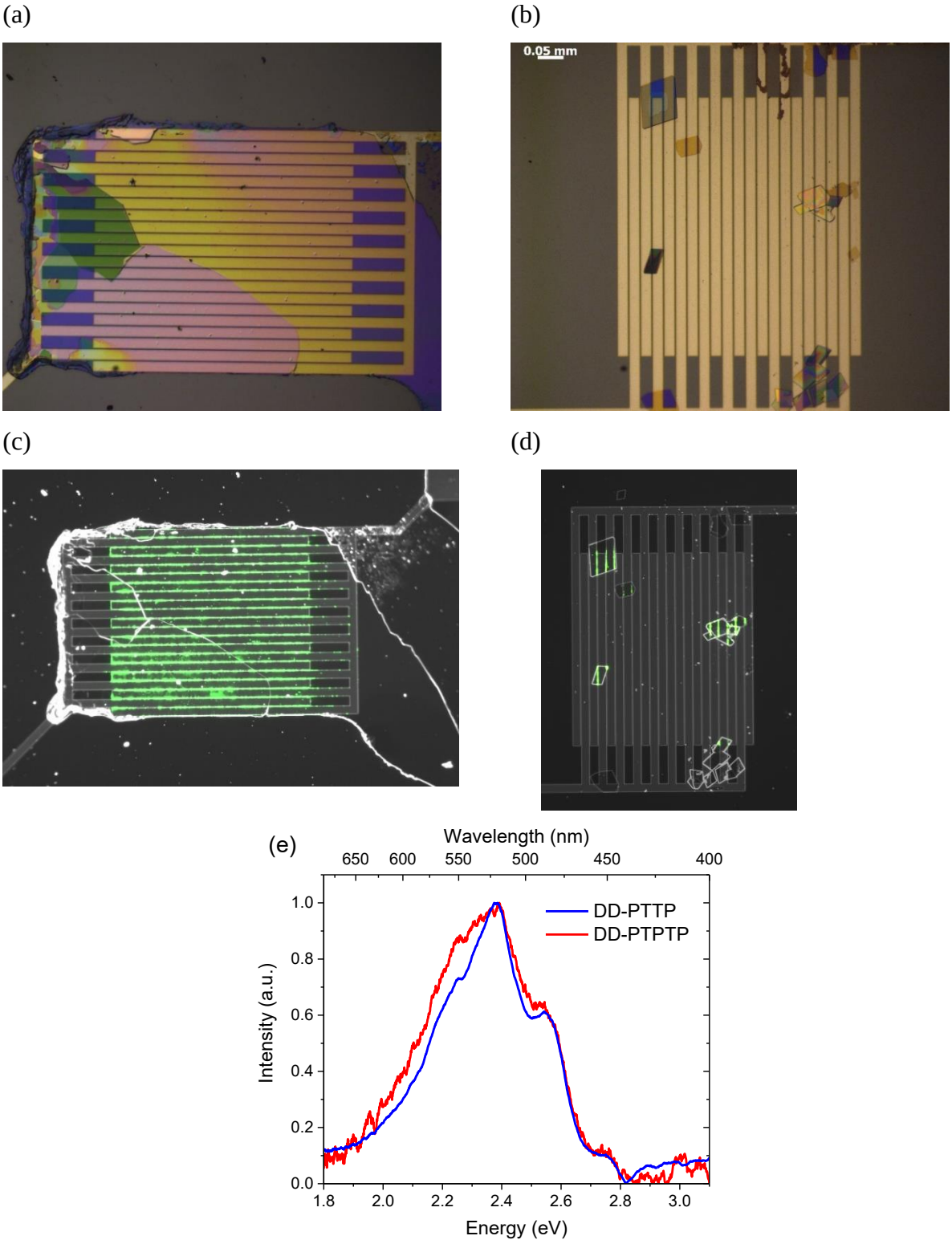

Figure S31. 3D SC OLETs. Optical microscopy images under backlight (a,b) and during the operation (c,d) for DD-PTTP (a,c) and DD-PTPTP (b,d), and EL spectra (e). The EL spectra show the less intensive red parts as compared with those of the PC OLETs (Fig. 15), which is naturally to assign to EL self-absorption. As the DD-PTTP crystals are thicker (several microns) than the DD-PTPTP (hundreds of nanometers) ones, the red part of the EL spectra is more suppressed by the EL self-absorption so that the EL spectra of both materials are nearly coincide in contrast with the EL spectra of the PC OLETs (Fig. 15).

9. References

1. J. Gierschner, J. Shi, B. Milián-Medina, D. Roca-Sanjuán, S. Varghese and S. Park, Luminescence in crystalline organic materials: from molecules to molecular solids, *Adv. Opt. Mater.*, 2021, **9**, 2002251.

2. L. G. Kudryashova, M. S. Kazantsev, V. A. Postnikov, V. V. Bruevich, Y. N. Luponosov, N. M. Surin, O. V. Borshchev, S. A. Ponomarenko, M. S. Pshenichnikov and D. Y. Paraschuk, Highly luminescent solution-grown thiophene-phenylene co-oligomer single crystals, *ACS Appl. Mater. Interfaces*, 2016, **8**, 10088-10092.

3. T. Y. Starikova, N. M. Surin, O. V. Borshchev, S. A. Pisarev, E. A. Svidchenko, Y. V. Fedorov and S. A. Ponomarenko, A novel highly efficient nanostructured organosilicon luminophore with unusually fast photoluminescence, *J. Mater. Chem. C*, 2016, **4**, 4699-4708.

4. S. J. Strickler and R. A. Berg, Relationship between absorption intensity and fluorescence lifetime of molecules, *J. Chem. Phys.*, 1962, **37**, 814-822.

5. O. D. Parashchuk, A. A. Mannanov, V. G. Konstantinov, D. I. Dominskiy, N. M. Surin, O. V. Borshchev, S. A. Ponomarenko, M. S. Pshenichnikov and D. Y. Paraschuk, Molecular self-doping controls luminescence of pure organic single crystals, *Adv. Funct. Mater.*, 2018, **28**, 1800116.

6. A. S. Davydov, Theory of molecular excitons, *Plenum Press, New York*, 1971.